

Weighted least-squares based control for a four axis gimbal set

Delano R. Carter^a, Patrick Duffey^a, Steve Bachorski^a, Martin Kägi^b, Howard Havlicsek^a

^aAcutronic USA Inc., 640 Alpha Drive, Pittsburgh, Pennsylvania 15238;

^bAcutronic Switzerland Ltd, Rosengartenstrasse 25, 8608 Bubikon, Switzerland

ABSTRACT

Gimbal lock is a phenomenon which occurs in multi-gimbaled systems when two axes are driven into a coplanar orientation, thereby resulting in the loss of one degree of rotational freedom. This paper presents a control scheme which introduces a redundant fourth axis in conjunction with an algorithm that minimizes weighted least-square gimbal rates, ultimately permitting the use of open inner and middle gimbals to achieve a wide field of view. The control algorithm produces a singularity/gimbal lock measure which is derived using the inner three gimbals, and used to adapt the weights and transition the table from three-axis operation to four-axis operation at or near the three-axis gimbal lock orientation. Weight adaptation minimizes the peak gimbal rate required to track a vehicle reference rate profile. The control strategy also minimizes tracking errors between vehicle kinematic motion, which is obtained from the vehicle dynamics simulation, and kinematic motion induced onto the table-mounted payload. The control algorithm accepts Euler angles and body rates, as defined in the body fixed frame of reference, and generates four gimbal command sets. Each gimbal command set consists of gimbal acceleration, rate, and angle. Mathematical analysis, simulation, and 3-D CAD multi-body dynamics visualizations are included, illustrating differences between desired vehicle kinematic motion and that induced by this control strategy onto the table mounted payload, including an examination of effects due to finite gimbal control loop bandwidths.

Keywords: gimbal lock, singularity, least-squares, adaptation, motion control, Euler angles, mathematical modeling, multi-body dynamics, flight motion simulator, kinematic motion

1. INTRODUCTION

Hardware-in-the-loop (HWIL) testing occurs between all software based system performance sizing and evaluation, and system level tests of fully integrated hardware. Hardware-in-the-loop simulators permit the performance evaluation of key guidance, navigation, and control system components in a controlled and repeatable environment. HWIL simulation consists of three major components: the hardware article under test, a flight motion simulator (FMS), and a command and control computer. The hardware test article is mounted to the flight motion simulator. The flight motion simulator induces kinematic motion onto its payload in a fashion that replicates the payload flight conditions. The command and control computer issues commands to the flight motion simulator and receives telemetry from the FMS mounted payload. The telemetry is processed in the command and control computer. High fidelity system modeling and simulation occurs in the command and control computer which simulates a real-world scenario. The result of the processed telemetry is issued to the FMS as kinematic motion commands for replicating the command-and-control-computer simulated flight vehicle kinematic motions onto the FMS mounted payload.

The FMS must accurately and transparently induce the commanded kinematic motions onto its payload. Otherwise, the realism of the HWIL simulation is degraded, thereby increasing the set of known unknowns when going from lab to operational environments. The reduction in this uncertainty set enhances the probability of success of operational system level tests. During actual operation, a flight vehicle has unrestricted kinematic motion about the three rotational degrees-of-freedom over a large operational envelope. To maintain this realism in the HWIL simulation environment, the FMS gimbal set must permit unrestricted motion of its payload about three rotational degrees-of-freedom.

Send correspondence to D.R.C., E-mail: dcarter@acutronic.com, Telephone: 1 412 427 2014

Gimbal lock is a state where the gimbal set is unable to produce kinematic motion in at least one degree of freedom. Near these states, three gimbal HWIL flight motion simulators attain high gimbal rates, even for benign commanded rate profiles, and degraded kinematic motion command tracking. This loss of command tracking is an artifact of the three gimbal HWIL flight motion simulator limitations and must be prevented from occurring during HWIL testing so as to not corrupt measured lab test results. The use of a four gimbal HWIL FMS precludes gimbal lock from occurring when implemented with the appropriate control strategy.

A four axis gimbal set control strategy based on minimizing the weighted least squares (wLS) of gimbal rates is considered. The weights are adapted in real time, based on gimbal set configuration, to minimize peak gimbal rates required to track commanded vehicle kinematic motion profiles. The four axis gimbal set consists of an ‘inner’ first gimbal, a ‘middle’ second gimbal, an ‘outer’ third gimbal, and a ‘base’ fourth gimbal. The base gimbal is initially redundant in orientation to the inner gimbal. The four axis gimbal set permits a wide field of view which requires open gimbals for the inner and middle gimbal axes (i.e. the smallest two axes).

This paper presents a methodology for controlling the four gimbal HWIL flight motion simulator to accurately induce onto the FMS mounted payload the commanded kinematic motions which are generated by the HWIL simulation command and control computer. In the remainder of this paper are Section 2 where three and four gimbal FMS kinematic motions are discussed, Section 3 which addresses the control of the four axis gimbal set, Section 4 which provides four gimbal FMS control simulation results, and Section 5 which states conclusions.

2. FLIGHT MOTION SIMULATOR KINEMATIC MOTION

The flight motion simulator receives its commands from a HWIL command and control computer. The command and control computer produces FMS commands through the use of high fidelity modeling and real-time simulation of flight vehicle dynamics. The FMS commands may consist of flight vehicle Euler angles, angular rates, and angular accelerations. The FMS controller then performs real-time conversion of these commands into gimbal commands so that the identical kinematic motion is induced onto the FMS payload in a transparent manner. The FMS kinematic motion commands may be converted into gimbal commands by mapping the angular acceleration and angular rate vectors into vehicle body frame coordinates. Ideally, the vehicle body frame coordinates are identical to the FMS payload frame coordinates. The gimbal rates are determined by mapping the payload commanded rates into gimbal rates. The gimbal acceleration may be found by taking the derivative of the gimbal rates. The gimbal angles may be found by integrating the gimbal rates. Initial FMS attitude is determined from the Euler angle commands. The following sections show the details of performing the conversion from FMS kinematic motion commands, as received from the command and control computer, to gimbal set kinematic motions for the three and four gimbal FMS.

2.1 Three Gimbal FMS

It is useful to begin by examining the three gimbal FMS kinematic motion generation since it is used within the four gimbal control strategy. The three gimbal set FMS consists of outer, middle, and inner gimbals. A three gimbal set visualization is given in the left panel of Figure 1. Each gimbal has attached to it a frame of reference. The gimbal fixed frames rotate with their respective gimbal. With the gimbal set at its (0,0,0) orientation, all gimbal fixed frames are aligned with the inertial frame of reference. At this gimbal set attitude, the inertial frame x-axis is collinear with the outer gimbal rotation axis, the inertial frame y-axis is collinear with the middle gimbal rotation axis, and the inertial frame z-axis is collinear with the inner gimbal rotation axis. The corresponding Euler angle/axis sequence is $(\phi, \theta, \psi)/(x, y, z)$. The elementary rotation transformations¹ applied in the development of the gimbal set coordinate transformation matrix, $T_{Body/Inertial}$, are

$$Rot_x(\sigma) = \begin{bmatrix} 1 & 0 & 0 \\ 0 & \cos \sigma & \sin \sigma \\ 0 & -\sin \sigma & \cos \sigma \end{bmatrix}, \quad Rot_y(\sigma) = \begin{bmatrix} \cos \sigma & 0 & -\sin \sigma \\ 0 & 1 & 0 \\ \sin \sigma & 0 & \cos \sigma \end{bmatrix}, \quad Rot_z(\sigma) = \begin{bmatrix} \cos \sigma & \sin \sigma & 0 \\ -\sin \sigma & \cos \sigma & 0 \\ 0 & 0 & 1 \end{bmatrix}$$

where σ represents an arbitrary rotation angle. The Euler angle/axis sequence requires the multiplication of the elementary rotational transformations in the order $Rot_z(\psi)Rot_y(\theta)Rot_x(\phi)$ to obtain $T_{Body/Inertial}$. This

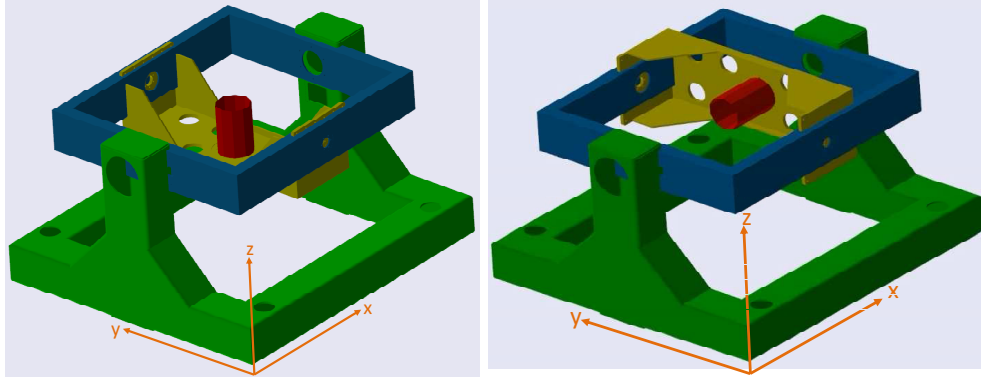


Figure 1. Three gimbal set showing inertial reference frame (left) and gimbal lock configuration (right).

coordinate frame transformation matrix is

$$T_{Inertial}^{Body} = \begin{bmatrix} \cos \theta \cos \psi & \cos \psi \sin \theta + \cos \phi \sin \psi & -\cos \phi \cos \psi \sin \theta + \sin \phi \sin \psi \\ -\cos \theta \sin \psi & \cos \phi \cos \psi - \sin \theta \sin \phi \sin \psi & \cos \psi \sin \phi + \cos \phi \sin \theta \sin \psi \\ \sin \theta & -\cos \theta \sin \phi & \cos \theta \cos \phi \end{bmatrix}. \quad (1)$$

The transformation matrix given in Equation 1 converts the acceleration and velocity vectors from inertial frame coordinates to body (payload) frame coordinates. Kinematic motions may be converted from body frame coordinates to inertial frame coordinates using the transpose of Equation 1, $T_{Body/Inertial}^T$.

We now examine the limitations imposed by a three axis gimbal set in tracking unrestricted kinematic motion about the three rotational degrees of freedom over a large operational envelope. An important FMS requirement is to accurately track kinematic motion commands produced by the command and control computer. For the following, the command and control computer simulated flight vehicle kinematic motion vectors are defined in the body fixed coordinate frame. These vectors can be transformed from inertial coordinates by using Equation 1. Using the vehicle kinematic motion vectors and Euler angles, which describe the attitude of the body coordinate frame with respect to the inertial reference frame, the required gimbal kinematics may be derived. The kinematic motions for the FMS gimbals are derived by determining the mapping matrix from Euler angle rates to body rates for the FMS and taking the inverse of the resultant mapping. The mapping matrix from Euler angle rates to body rates is a function of the FMS gimbal rotation sequence. For the three gimbal FMS under consideration, the mapping from Euler angle rates to body rates is determined as

$$\begin{aligned} \omega_{Body}^{Body} &= Rot_z(\psi)Rot_y(\theta)Rot_x(\phi)[\dot{\phi}, 0, 0]^T + Rot_z(\psi)Rot_y(\theta)[0, \dot{\theta}, 0]^T + Rot_z(\psi)[0, 0, \dot{\psi}]^T \\ &= \begin{bmatrix} \cos \theta \cos \psi & \sin \psi & 0 \\ -\cos \theta \sin \psi & \cos \psi & 0 \\ \sin \theta & 0 & 1 \end{bmatrix} \begin{bmatrix} \dot{\phi} \\ \dot{\theta} \\ \dot{\psi} \end{bmatrix} \\ &= \Lambda \dot{\gamma} \end{aligned}$$

where ω_{Body}^{Body} denotes the body angular rate vector ω with coordinates in the body reference frame. The required gimbal rates may be determined by taking the inverse of Λ and computing

$$\dot{\gamma} = \Lambda^{-1} \omega_{Body}^{Body}$$

with

$$\Lambda^{-1} = \frac{1}{\cos \theta} \begin{bmatrix} \cos \psi & -\sin \psi & 0 \\ \sin \psi \cos \theta & \cos \psi \cos \theta & 0 \\ -\cos \psi \sin \theta & \sin \psi \sin \theta & \cos \theta \end{bmatrix} = \begin{bmatrix} \cos \psi \sec \theta & -\sin \psi \sec \theta & 0 \\ \sin \psi & \cos \psi & 0 \\ -\cos \psi \tan \theta & \sin \psi \tan \theta & 1 \end{bmatrix}.$$

The inverse, Λ^{-1} , exists only at points where the determinant of Λ is nonzero, (i.e. $\Delta(\Lambda) \neq 0$). Since $\Delta(\Lambda) = \cos \theta$, then Λ is invertible for all $\theta \neq n\pi/2, n = \pm 1, \pm 3, \dots$. The values of θ for which the inverse does not exist

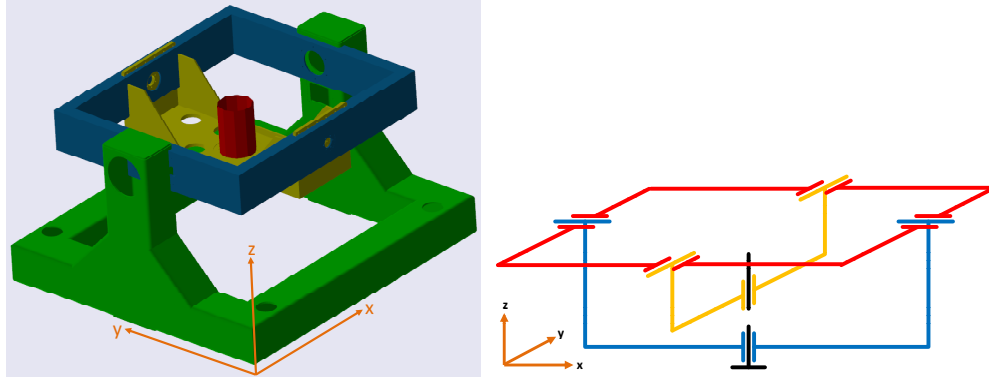


Figure 2. Four gimbal set (left) and rotation axes diagram (right) showing inertial reference frame.

correspond to gimbal set configurations that have the inner gimbal rotation axis collinear with the outer gimbal rotation axis as shown in the right panel of Figure 1. For this configuration, the three gimbal set FMS is unable to produce kinematic motion about the inertial frame z-axis, neither can the gimbal set create torque about this axis. Not only are singular configurations such as $\theta = n\pi/2, n = \pm 1, \pm 3, \dots$ problematic, but so is operation in the neighborhood of these singular configurations. Kinematic motion in the vicinity of singular configurations requires high gimbal rates to track even small rates about the inertial frame z-axis. This condition results in inaccurate kinematic motion tracking of the FMS mounted payload relative to the command and control computer commanded kinematic motions. A loss in realism is then encountered during the HWIL simulation scenario that is exclusively the result of lab equipment hardware limitations that does not exist during real world applications.

2.2 Four Gimbal FMS

To better emulate the singularity-free real-world operation of the flight vehicle envelope of interest, we introduce a fourth gimbal. The over-actuated system provides the opportunity to avoid the gimbal lock configuration previously discussed. It is beneficial to have this fourth gimbal active within some enlarged neighborhood about the singular configurations. The size of this neighborhood will influence the peak rate and power demand of the gimbal set; enlarging this neighborhood reduces peak rate and acceleration demands on the gimbals. The wLS algorithm discussed Section 3 provides a means for tuning the neighborhood size about the singular configurations for activating the fourth gimbal.

The nomenclature and alignment of the inner three gimbals are as given in Section 2.1 for the four gimbal set. The four gimbal set rotation axes are displayed in the right panel of Figure 2. Even though the fourth gimbal is not explicitly depicted in the left panel of Figure 2, the right panel makes clear that the fourth gimbal is attached to the base of the three gimbal set, hence the designation base gimbal. The base gimbal is configured so that its rotational axis is collinear with the inner gimbal rotation axis at the $(0, 0, 0, 0)$ gimbal set configuration. This corresponds to having the base gimbal rotational axis collinear with the inertial frame z axis. The rotation angle/axis sequence is $(\alpha, \phi, \theta, \psi)/(z, x, y, z)$. The coordinate frame transformation matrix for the four gimbal set follows from the multiplication of the elementary rotational transformations in the order $Rot_z(\psi)Rot_y(\theta)Rot_x(\phi)Rot_z(\alpha)$ and is

$$T_{Inertial}^{Body} = \begin{bmatrix} C\alpha C\theta C\psi - S\alpha(C\psi S\theta S\phi + C\phi S\psi) & C\theta C\psi S\alpha + C\alpha(C\psi S\theta S\phi + C\phi S\psi) & -C\phi C\psi S\theta + S\phi S\psi \\ -C\phi C\psi S\alpha + (-C\alpha C\theta + S\alpha S\theta S\phi)S\psi & C\alpha C\phi C\psi - (C\theta S\alpha + C\alpha S\theta S\phi)S\psi & C\psi S\phi + C\phi S\theta S\psi \\ C\alpha S\theta + C\theta S\alpha S\phi & S\alpha S\theta - C\alpha C\theta S\phi & C\theta C\phi \end{bmatrix} \quad (2)$$

where $C\alpha = \cos \alpha$, $S\alpha = \sin \alpha$, and so forth. The mapping matrix from body rotational kinematic motion to gimbal kinematic motion is derived in an analogous manner as for the three gimbal set in Section 2.1. The

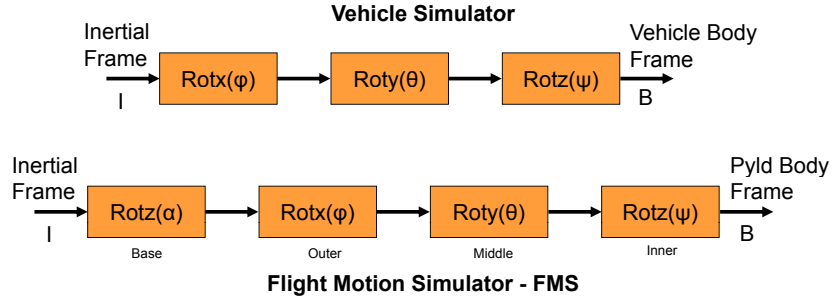


Figure 3. Vehicle and flight motion simulator Euler axis and angle sequences. The FMS mounted payload must track, in real time, the vehicle body frame resulting from the vehicle simulator.

mapping from gimbal rates to body rates is

$$\begin{aligned}
 \omega_{Body}^{Body} &= Rot_z(\psi)Rot_y(\theta)Rot_x(\phi)Rot_z(\alpha)[0, 0, \dot{\alpha}]^T + Rot_z(\psi)Rot_y(\theta)Rot_x(\phi)[\dot{\phi}, 0, 0]^T \\
 &\quad + Rot_z(\psi)Rot_y(\theta)[0, \dot{\theta}, 0]^T + Rot_z(\psi)[0, 0, \dot{\psi}]^T \\
 &= \begin{bmatrix} -\cos \phi \cos \psi \sin \theta + \sin \phi \sin \psi & \cos \theta \cos \psi & \sin \psi & 0 \\ \cos \psi \sin \phi + \cos \phi \sin \theta \sin \psi & -\cos \theta \sin \psi & \cos \psi & 0 \\ \cos \theta \cos \phi & \sin \theta & 0 & 1 \end{bmatrix} \begin{bmatrix} \dot{\alpha} \\ \dot{\phi} \\ \dot{\theta} \\ \dot{\psi} \end{bmatrix} \\
 &= A\dot{\delta}.
 \end{aligned} \tag{3}$$

where A is the four gimbal set Jacobian matrix. With this gimbal set configuration, as the middle axis rotates some odd multiple of 90 degrees, as done before, there is still the capability of applying an inertial z-axis kinematic motion component utilizing the base gimbal. For the flight vehicle envelope of interest in this paper, this is sufficient for attaining the HWIL simulation realism desired. However, note that this four gimbal set arrangement has a gimbal lock configuration of its own. It occurs for the middle axis being at some odd multiple of 90 degrees and the outer axis at some odd multiple of 90 degrees. At these configurations, the four axis gimbal set is incapable of applying kinematic motion about the inertial frame y-axis. This is not a configuration that is encountered during the vehicle operational flight regime and will not be discussed further.

A visualization of the elementary rotation matrices composing Equation 2 is shown in Figure 3. Also displayed in Figure 3 are the elementary rotation matrices composing the vehicle coordinate frame transformation matrix. The four axis gimbal set and controller are deemed to be successfully implemented when the FMS mounted payload body frame accurately tracks the vehicle body frame. The vehicle body frame is computed in the command and control computer.

3. FOUR-AXIS FMS CONTROL STRATEGY AND ALGORITHM

The mapping matrix from four gimbal rates to three body rates is an underdetermined system of equations as demonstrated by Equation 3. There is then a multitudinous set of gimbal rates that map into a given set of body rates. There also is no solution for mapping a given set of body rates into a unique set of gimbal rates.

3.1 Control Strategy

To facilitate the mapping from body rates to a unique set of gimbal rates, the constraint that the weighted minimum two-norm solution of gimbal rates be enforced was adopted. Mathematically the problem is described as

$$\min_{\delta} \{\dot{\delta}^T Q \dot{\delta}\}$$

subject to $A\dot{\delta} = \omega$ where $\dot{\delta}$ = gimbal rates, ω = vehicle body rates, A = Jacobian matrix, and $Q = Q^T > 0$ is a positive definite weighting matrix. A solution^{2,3} to this problem statement is

$$\dot{\delta} = A^{\#}\omega$$

$$A^\# = Q^{-1} A^T [A Q^{-1} A^T]^{-1}$$

$$Q = \text{diag}(\rho_1, \rho_2, \rho_3, \rho_4), \quad \rho_n > 0$$

where $\text{diag}(\cdot)$ forms a diagonal matrix from its arguments, ρ_1 weights the authority of the base gimbal, ρ_2 weights the authority of the outer gimbal, ρ_3 weights the authority of the middle gimbal, and ρ_4 weights the authority of the inner gimbal. The weight ρ_1 is updated adaptively as a function of the nearness to gimbal lock of the inner three FMS gimbals. During periods in which the inner three gimbal set is not in the neighborhood of gimbal lock, the weight ρ_1 is made large to preclude motion of the base gimbal. The three gimbal configuration is useful because it requires less power and is advantageous for replicating simulation runs. Three gimbal operation is maintained until the inner three gimbals approach gimbal lock. To prohibit excessive rates during the excursion toward gimbal lock, the weight ρ_1 is reduced substantially in some acceptable neighborhood around gimbal lock. This weight reduction in ρ_1 allows the base gimbal to become active permitting accurate kinematic motion tracking in the vicinity of gimbal lock without encountering excessive gimbal rates. The metric used to indicate the onset of gimbal lock is the inner three gimbal set determinant, $\Delta(\Lambda) = \cos \theta$. As the determinant decreases below some threshold value, the weight on the base gimbal is correspondingly decreased, thereby activating the base gimbal. The peak rate required to track the kinematic motion profile in the vicinity of gimbal lock is reduced significantly by this mode of operation. As the inner three gimbals transit away from a gimbal lock configuration, the base gimbal weight is correspondingly increased, based on the singularity metric; reestablishing three gimbal set operation.

3.2 Control Algorithm

The four gimbal FMS mitigates the deleterious effects of gimbal lock that occurs for the three gimbal configuration when its middle axis is at odd multiples of 90 degrees. The weighted minimum two-norm of gimbal rates is the controls solution applied for coordinating the four gimbal FMS motion. It allows accurate kinematic motion profiles to be induced onto the FMS payload, even for FMS configurations that would result in gimbal lock for the three axis system. The control algorithm can be summarized as follows:

1. Initialize FMS attitude using the command and control computer provided initial Euler angles
2. Induce matching kinematic motion onto FMS payload using vehicle rate data from the command and control computer
3. Rely on inner axis to induce required rates onto FMS payload relative to remaining axes by appropriate weighting
4. Operate FMS in three gimbal configuration when away from gimbal lock condition to reduce power usage
5. Activate base gimbal when near gimbal lock condition to keep peak rates low
6. Validate fidelity of induced FMS payload motion using command and control computer provided Euler angles and vehicle acceleration data

The control algorithm seeks to minimize error between the commanded and induced FMS payload kinematic motions while concurrently maintaining the set of gimbal rates low. The wLS based controls algorithm signal flow diagram used to accomplish this is displayed in Figure 4. This figure reveals that the overarching algorithm objective is to achieve $(\theta, \omega, \alpha)_{cmd}^T = (\theta, \omega, \alpha)_{actual}^T$, where $(\theta, \omega, \alpha)_{cmd}^T$ is from the command and control computer, and $(\theta, \omega, \alpha)_{actual}^T$ is the induced kinematic motion on the FMS payload. The Interface Translator algorithm has as its inputs the command and control computer output signals. It does the necessary processing to ensure that the input to the Steering Logic algorithm is the vehicle rate in the body reference frame. The translator also derives the initial FMS attitude vector. The Steering Logic algorithm accepts Euler angles and body rates and generates gimbal rate commands and the singularity (gimbal lock) metric as outputs. The algorithm utilizes the singularity measure to transition the four gimbal set arrangement from three gimbal operation to four gimbal operation at and near the inner three axis gimbal lock orientation. The FMS Command Generator transforms the initial attitude and gimbal rate commands into four gimbal command sets. Each set consists of gimbal acceleration, rate, and angle and are sent to the four gimbal FMS by way of the FMS controller. The FMS controller ensures that the FMS induces the required kinematic motions onto its payload.

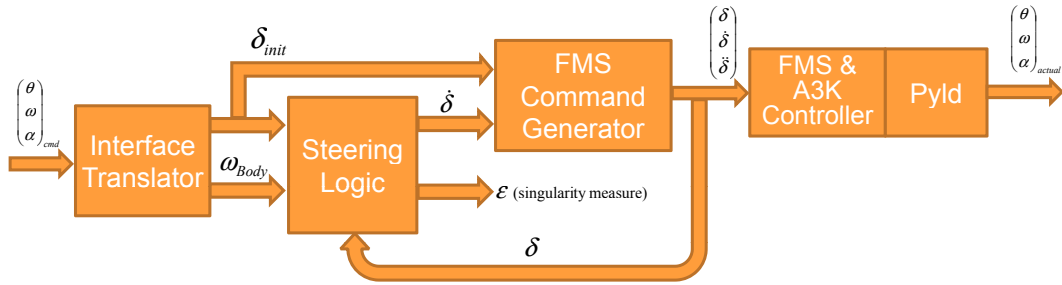


Figure 4. Four gimbal set control algorithm signal flow.

4. MODELING AND SIMULATION

A numerical math model was developed and simulations performed to analyze and verify the satisfactory operation of the control algorithm. The model was developed in the Matlab/SimMechanics⁴ environment. Simulation runs were conducted that included operation at and near the gimbal lock configuration. The impact of control loop bandwidth was examined by comparing the ideal bandwidth results to those obtained using a realistic bandwidth value. The measure of performance is how accurately the FMS induced motion on the payload tracks that of the simulated vehicle motion.

4.1 Model Description

The analysis model consists of three primary simulation components: the vehicle model component, the Transformation Computer component, and the four gimbal FMS and Acutrol3000 controller component. The vehicle model component simulates, at a very simplistic level, the command and control computer generated flight vehicle kinematic motions. The model consists of vehicle mass properties, gyro-dynamics, and torque actuators for simulating a three degree-of-freedom rotational motion profile. Three torque actuators apply torque to the vehicle relative to either inertial or body fixed frames of reference. The vehicle attitude is represented using a quaternion. The outputs from this simulation component are vehicle accelerations, rates, and angles with respect to the inertial and body frames of reference. According to Figure 4, this corresponds to signal $(\theta, \omega, \alpha)^T_{cmd}$. The vehicle rate vector, in body coordinates, is supplied as inputs to the Transformation Computer simulation component.

The Transformation Computer simulation component consists of the two blocks labeled Interface Translator and Steering Logic in Figure 4. This component implements the control algorithm described in Section 3.2. The Transformation Computer component models the real-time processing of the FMS Jacobian, the computation of FMS attitude nearness to gimbal lock, and the relative weightings of the gimbal commanded rates. The Transformation Computer converts the four-gimbal angle commands and the vehicle body rate vector command into FMS gimbal rate commands; this corresponds to $(\dot{\delta} = [\dot{\alpha}, \dot{\phi}, \dot{\theta}, \dot{\psi}]^T)$ in Figure 4. The gimbal rate commands are then issued to the Acutrol3000 controller simulation component as inputs.

The four gimbal FMS and Acutrol3000 controller simulation component consists of the blocks labeled FMS Command Generator, FMS & A3K Controller, and Pyld in Figure 4. This component models the application of control torques used for inducing the commanded kinematic motions onto the FMS payload, the four gimbal set rigid body gyro-dynamics, and the gimbal axis control loop dynamics. The gimbal axis nomenclature is: Base - α gimbal; Outer - ϕ gimbal; Middle - θ gimbal; and Inner - ψ gimbal. The Acutrol3000 controller completes the kinematic motion command set by coherently and synchronously synthesizing the gimbal acceleration command vector, $(\ddot{\delta} = [\ddot{\alpha}, \ddot{\phi}, \ddot{\theta}, \ddot{\psi}]^T)$, and the gimbal angle command vector, $(\delta = [\alpha, \phi, \theta, \psi]^T)$, from the gimbal rate command vector, $(\dot{\delta} = [\dot{\alpha}, \dot{\phi}, \dot{\theta}, \dot{\psi}]^T)$. These gimbal commands are issued to the Acutrol3000 motion controller control loops. The Acutrol3000 motion controller provides independent articulation control of each gimbal axis. This is performed using rate control loops, position control loops, and gimbal rate and acceleration command feed-forwards. The FMS actuators are electric motors with co-located sensors providing relative gimbal angle measurements for feedback. The actual gimbal rate and acceleration states are estimated using the Acutrol3000

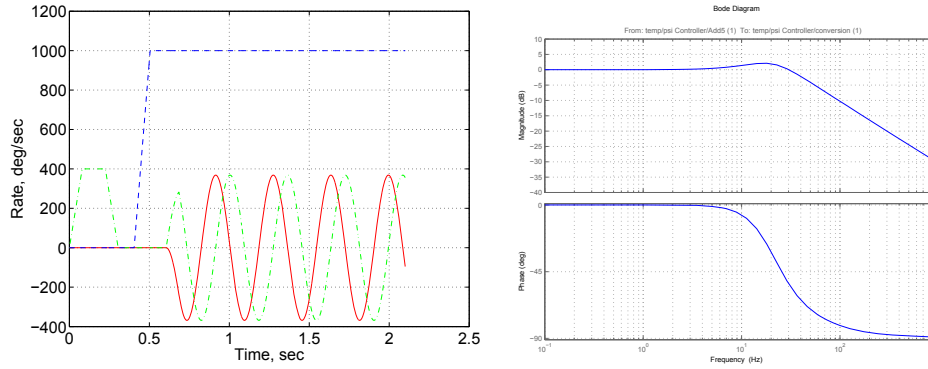


Figure 5. [Left Panel] Vehicle body rates, measured in body coordinate frame, from vehicle simulator model (i.e. Command Profile). Legend (left): Red Solid (X-axis), Green Dash-Dot (Y-Axis), Blue Dash (Z-axis). [Right Panel] Control loop frequency response for each gimbal axis.

state observer. The FMS payload attitude is represented using a quaternion. The outputs from this simulation component are payload accelerations, rates, and angles with respect to the inertial and the body frames of reference; this corresponds to $(\theta, \omega, \alpha)_{actual}^T$ in Figure 4. The payload rate vector, in body coordinates, is compared against that of the vehicle simulation component for performance assessment.

4.2 Simulation Results

A four gimbal set controller simulation was performed to ascertain the control algorithm performance presented in Section 3.2. To accomplish this, multiple scenarios were simulated using different kinematic motion vectors from the flight vehicle simulator component. Two simulation scenarios are included in this section. The first scenario simulates flight vehicle coning kinematic motion, induced by gyroscopic coupling, in the vicinity of gimbal lock. For this first scenario, two simulations were performed. The first simulation assumes a wide-bandwidth control loop for each axis, corresponding to an ideal mechanically stiff system design. The result verifies the control algorithm implementation and establishes theoretical performance bounds. The second simulation uses a control loop with 35 Hz bandwidth for each axis, corresponding to practical limitations within which a motion simulator must operate. The result demonstrates the effects of gimbal bandwidth on system performance.

The second scenario simulates a constant acceleration through gimbal lock while maintaining a sinusoidal motion in inertial space. It exercises the base gimbal activation and deactivation in the neighborhood of gimbal lock. The control loop bandwidths are set to 35Hz. The second scenario was applied to the three gimbal set, as well as to the four gimbal set, for performance comparison.

4.2.1 Gyroscopic Kinematic Motion Near Gimbal Lock

The vehicle kinematic motion profile used for this scenario is shown in the left panel of Figure 5. This vehicle profile starts at its $(0, 0, 0)$ Euler angle configuration; that is, the vehicle body frame is co-aligned with the inertial frame. The vehicle then rotates 90 degrees about the inertial y-axis. This is seen as the 400 deg/sec trapezoidal ramp profile displayed as green dash-dot in Figure 5. This maneuver places the inner three gimbal set into a gimbal lock configuration. Once the 90 deg vehicle motion is complete, the vehicle begins to rotate about the inertial space x-axis up to 1000 deg/sec. This is displayed by the blue dash trace in Figure 5. After the vehicle is stabilized at this spin rate, an inertial space rate about the y-axis is commanded. Due to gyroscopic coupling, a sinusoidal motion about the x- and y-axes results as shown in Figure 5. The motion occurs in the neighborhood of gimbal lock for the inner three axis gimbal set. This vehicle kinematic motion profile was used to assess the performance of the four gimbal set control algorithm. A primary performance goal for the control algorithm is to have the FMS mounted payload track the vehicle kinematic motion with insignificant error. The resultant tracking errors are given in Figure 6. These are satisfactory results because the tracking errors are acceptably low. This verifies the logic and implementation of the four gimbal set control algorithm. The Figure 6 results were obtained using ideal (stiff) gimbal control loop bandwidths.

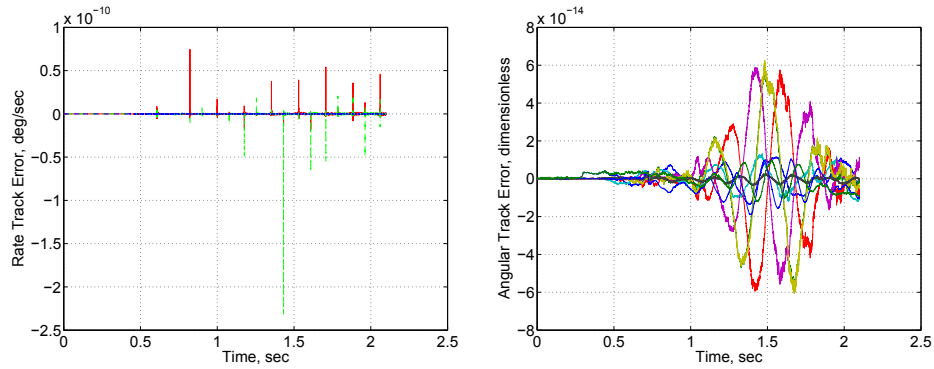


Figure 6. FMS payload rate (left) and angle (right) tracking error with respect to flight vehicle kinematic motion using ideal (stiff) bandwidths. Legend (left): Red Solid (X-axis), Green Dash-Dot (Y-Axis), Blue Dash (Z-axis). Legend (right): Nine traces representing body frame rotation matrix difference.

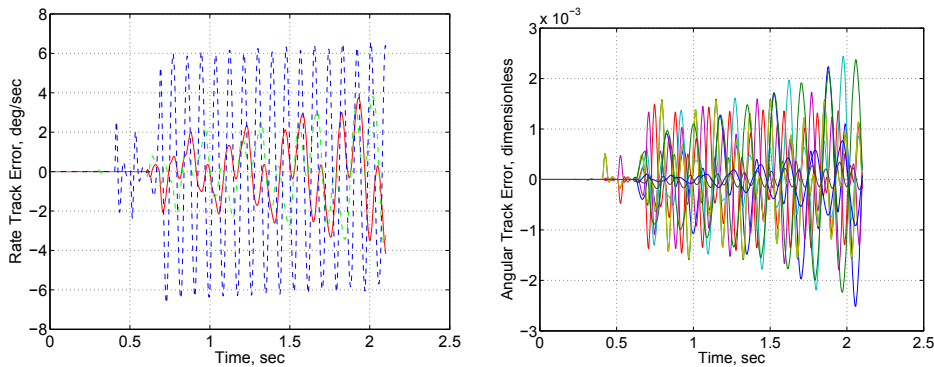


Figure 7. FMS payload rate (left) and angle (right) tracking error with respect to flight vehicle kinematic motion using 35 Hz bandwidths. Legend (left): Red Solid (X-axis), Green Dash-Dot (Y-Axis), Blue Dash (Z-axis). Legend (right): Nine traces representing body frame rotation matrix difference.

Next, we examine the impact that lower control loop bandwidths incur. The same kinematic motion profile given in Figure 5 was used for this purpose. The gimbal control loop bandwidths were set to 35 Hz for all four gimbal axes. This produced the results depicted in Figure 7. As expected, the tracking errors are larger but not unacceptably so. The control loop frequency response used to generate this result is shown in the right panel of Figure 5.

4.2.2 Sine Wave Kinematic Motion Through Gimbal Lock

For this simulation run, the vehicle kinematic motion consisted of two simultaneously implemented motion components throughout the run. One motion component consisted of a constant acceleration about the inertial space y-axis. The second motion component was a predominant sinusoidal vehicle motion about the inertial space z-axis. The left panel of Figure 8 shows the motion. This is a motion profile that the inner three gimbal set is unable to follow alone. For the four gimbal FMS payload to track this motion, it is required that the base gimbal become active to maintain the inertial z-axis sinusoidal motion as the inner three gimbal set traverses near and through gimbal lock configuration. The FMS payload tracking will be assessed while traversing through the gimbal lock configuration.

During the course of this run, the singularity metric achieved the profile given in the right panel of Figure 8. The red solid trace goes to zero where the inner three gimbal axes are at gimbal lock. The four gimbal set is controlled to maintain singularity free behavior by activating the base gimbal near the inner three-axis gimbal lock configuration. The commanded and replicated vehicle motion is depicted in Figure 9. The vehicle motion in body coordinates is displayed in the left panel. The right panel displays the induced motion onto the FMS

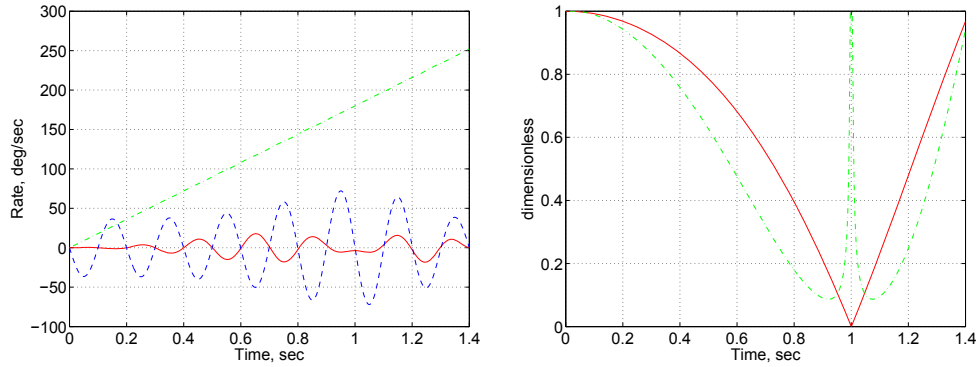


Figure 8. Four gimbal set results. [Left Panel] Vehicle rates, measured in inertial coordinate frame, from vehicle simulator model (i.e. Command Profile). Legend: Red Solid (X-axis), Green Dash-Dot (Y-Axis), Blue Dash (Z-axis). [Right Panel] Singularity metrics: Three gimbal system (Red Solid), Four gimbal system (Green Dash-Dot).

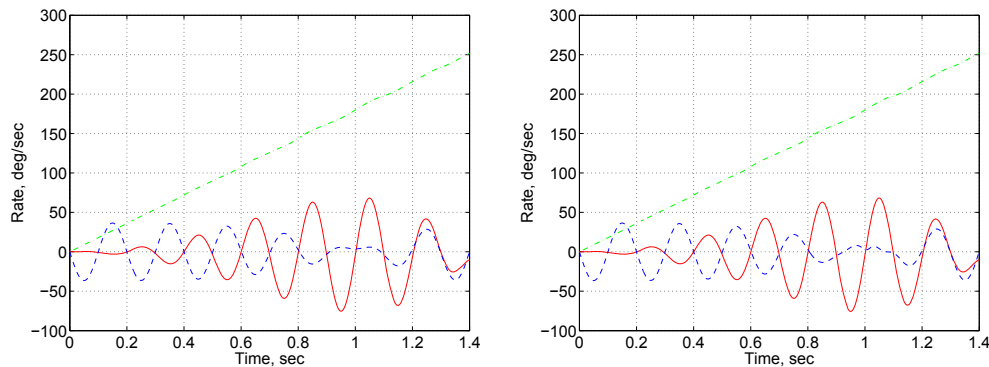


Figure 9. Four gimbal set results. Commanded (left) and replicated (right) vehicle motion in body frame coordinates. Legend: Red Solid (X-axis), Green Dash-Dot (Y-Axis), Blue Dash (Z-axis).

payload. These results were obtained using a 35 Hz control loop bandwidth as shown in Figure 5 for all gimbal axes. The tracking error between these two is presented in Figure 10. The tracking rate error plot shows some degradation in tracking as the gimbal lock configuration is traversed, but overall the results are adequate.

The base gimbal activation setting is adjustable. For this simulation run, the base gimbal activation occurred about a small neighborhood of the gimbal lock state. This resulted in fast transients for the base gimbal as it transitioned from its inactive to active state. The control loop bandwidth filtered some of these fast transient effects, thereby inducing the tracking error displayed in Figure 10. The right panel of Figure 10 shows the gimbal rates for this simulation run. Of special note is the base gimbal motion, displayed as red solid. This plot shows the base gimbal remains essentially inactive until the inner three-axis set neighborhood of gimbal lock is entered. This occurs around 0.4 seconds on this plot. Even so, this gimbal axis remains relatively benign until around 0.8 seconds at which time the base gimbal rapidly assumes the responsibility for generating the sinusoidal motion about the inertial space z-axis. This assumption of responsibility is terminated around 1.2 seconds as the inner three-axis set moves away from its gimbal lock configuration. The times 0.8 and 1.2 seconds on the gimbal rate plot shown in Figure 10 correspond approximately to a value of 0.4 on the singularity metric plot (red solid trace) displayed in Figure 8. Below this value the base gimbal is made fully active. The base gimbal response may be tailored by appropriate shaping of the base gimbal weighting function.

It is informative to compare the three gimbal set results to the four gimbal set results just presented. Setting the base gimbal weight large constrains the base gimbal motion. To demonstrate three gimbal set only behavior, we heavily weight the base gimbal to prohibit its activation. The singularity metric, vehicle and payload rates, rate track error, and gimbal rates are of primary interest for performing this comparison. The three gimbal set

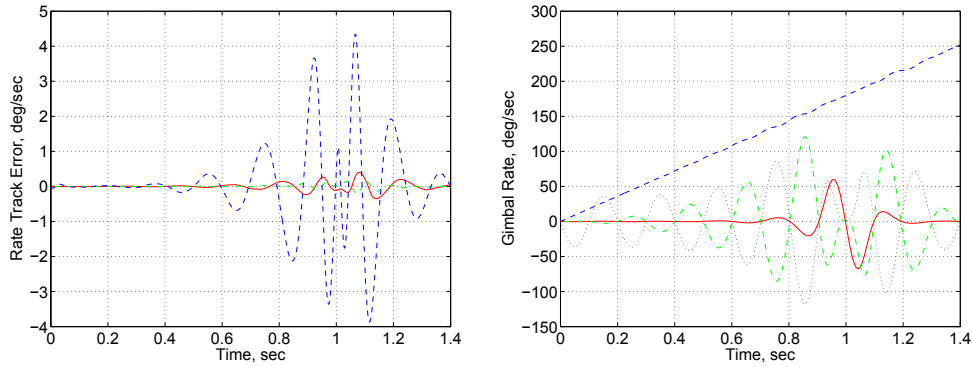


Figure 10. Four gimbal set results. [Left Panel] Tracking rate error. Legend: Red Solid (X-axis), Green Dash-Dot (Y-Axis), Blue Dash (Z-axis). [Right Panel] Commanded gimbal rates. Legend: Red Solid (Base), Green Dash-Dot (Outer), Blue Dash (Middle), Black Dot (Inner).

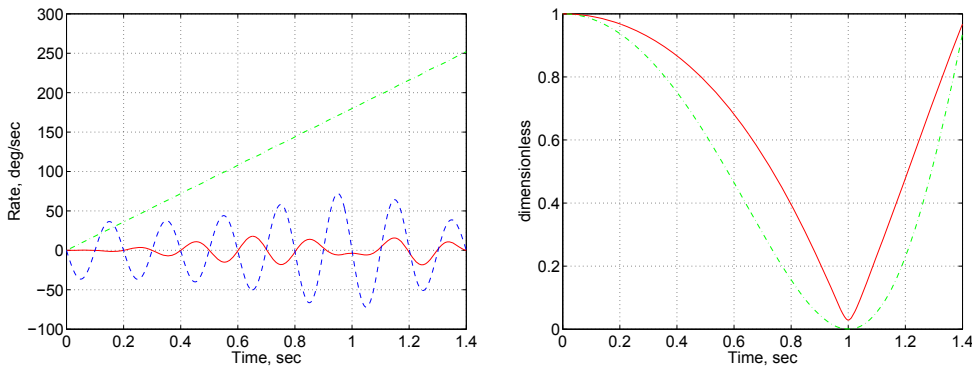


Figure 11. Three gimbal set results. [Left Panel] Vehicle rates, measured in inertial coordinate frame, from vehicle simulator model (i.e. Command Profile). Legend: Red Solid (X-axis), Green Dash-Dot (Y-Axis), Blue Dash (Z-axis). [Right Panel] Singularity metrics: Three gimbal system (Red Solid), Four gimbal system (Green Dash-Dot).

command profile is identical to the profile used for the four gimbal set. The three gimbal set command profile and singularity metric are displayed in Figure 11. The commanded and induced body rates are depicted in Figure 12. The accompanying rate track errors and gimbal rates are shown in Figure 13. A comparison of the three gimbal set results (Figures 11-13) to those obtained for the four gimbal set (Figures 8-10) reveals the three gimbal set poor performance in the neighborhood of gimbal lock. As seen in Figure 13, the three gimbal set exhibits loss of rate command tracking that is accompanied by excessively large rate commands as the singular configuration is approached. The corresponding plots for the four gimbal system, Figure 10, shows superior system performance near the singular configuration.

5. CONCLUSIONS

The weighted least squares based control for a four axis gimbal set successfully tracks commanded kinematic motions over a larger operational envelope than is achievable for a three axis gimbal set. This enhances the realism of HWIL simulation environments. Mathematical analysis, modeling, and simulation were used to demonstrate the larger operational envelope capability. Mathematical analysis identified gimbal lock as the root cause for limiting the performance envelope of a three axis gimbal set. It results from the Jacobian matrix determinant going to zero. The kinematic equations for the over-actuated four axis gimbal set were shown not to have this invertibility limitation. However, selection of a gimbal rate command vector based on a given body rate command vector is not unique. Employing the weighted least squares of gimbal rates constraint makes this selection unique. Modeling and simulation results showed the successful operation of the wLS control algorithm in the neighborhood of gimbal lock. There is a trade-off between gimbal control system bandwidth

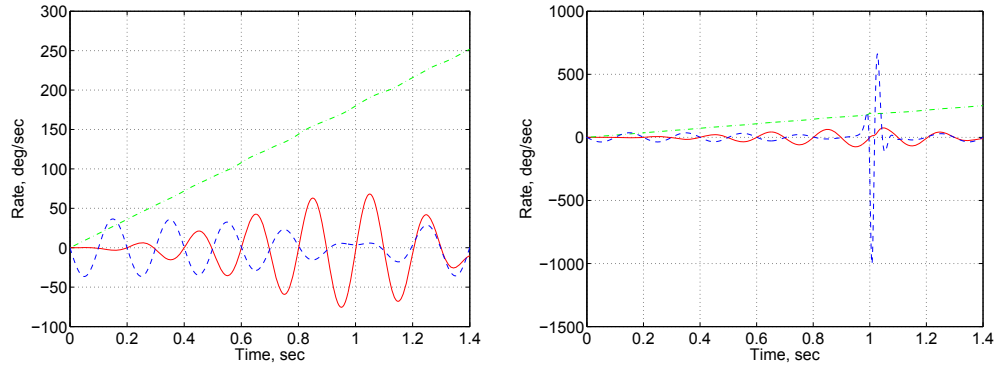


Figure 12. Three gimbal set results. Commanded (left) and replicated (right) vehicle motion in body frame coordinates. Legend: Red Solid (X-axis), Green Dash-Dot (Y-Axis), Blue Dash (Z-axis).

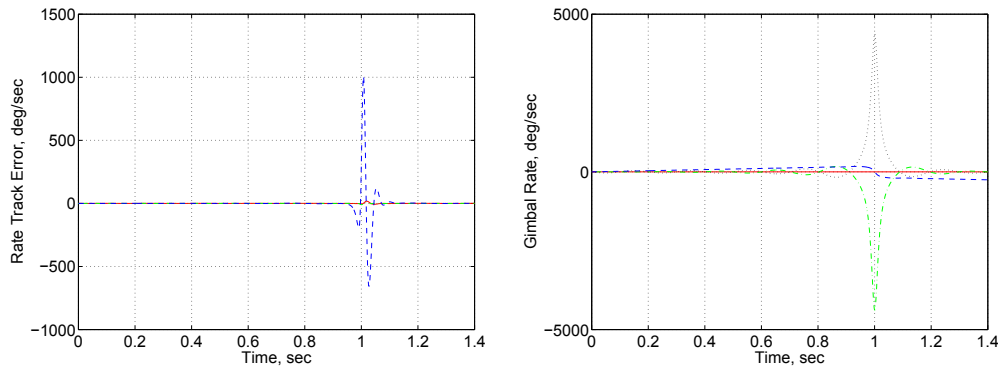


Figure 13. Three gimbal set results. [Left Panel] Tracking rate error. Legend: Red Solid (X-axis), Green Dash-Dot (Y-axis), Blue Dash (Z-axis). [Right Panel] Commanded gimbal rates. Legend: Red Solid (Base), Green Dash-Dot (Outer), Blue Dash (Middle), Black Dot: (Inner).

and base gimbal activation domain size. Activation start within a small neighborhood about gimbal lock may require fast transients for the base gimbal. The gimbal control system bandwidth may filter these transients thereby impacting FMS command tracking performance. The control system bandwidth and adaptive weighting functions can be shaped to operate synergistically to attain small track error and reasonable gimbal rates based on the FMS overarching system requirements. The wLS control algorithm transitions the four gimbal set from four gimbal operation to three gimbal operation and vice-versa automatically by adapting gimbal weights in real time. Results showed that a three gimbal set exhibited poor tracking and excessive gimbal rates in the neighborhood of gimbal lock. The wLS control algorithm showed superior performance in the same neighborhood about gimbal lock with small command track errors and reasonable gimbal rates. The gimbal rate weighting matrix may be tuned so that lower inertia axes (i.e. lower power) provide the majority of the commanded payload rate as a function of the four gimbal set configuration.

REFERENCES

- [1] Kuipers, J. B., [*Quaternions and Rotation Sequences*], Prentice University Press, Princeton, NJ (1999).
- [2] Wie, B., Heiberg, C., and Bailey, D., "Singularity robust steering logic for redundant single-gimbal control moment gyros," *Journal of Guidance, Control, and Dynamics* **24**, 865–872 (2001).
- [3] Noble, B. and Daniel, J. W., [*Applied Linear Algebra*], Prentice-Hall, Englewood Cliffs, NJ, third ed. (1988). 346-350.
- [4] Wood, G. D. and Kennedy, D. C., "Simulating mechanical systems in Simulink with SimMechanics," Tech. Rep. 91124v00, The Mathworks, 3 Apple Hill Drive, Natick, MA. www.mathworks.com.